CHAPTER V

NANOSTRUCTURED MIXED OXIDES AS GAS SENSORS FOR CARBON MONOXIDE (CO) MONITORING

5.1 Abstract

Nanostructured powders of Nb-doped TiO_2 (TN) and SnO_2 mixed with Nb-doped TiO_2 in two 2 different atomic ratios: 10 to 1 (TSN 101) and 1 to 1 ratio (TSN 11), were synthesized using reverse micelle microemulsion of nonionic surfactant (brine solution/1-hexanol/Triton X-100/cyclohexane). The powders were characterized by transmission electron microscopy (TEM), X-ray diffractometry (XRD) and BET surface area analysis. Thick films were fabricated for gas sensors and characterized by XRD and field emission scanning electron microscopy (FE-SEM). The effect of the film morphology and firing temperature on CO sensitivity was studied. The gas response of TSN 11 was clearly higher (about 11) than that obtained with TN and TSN 101. The firing temperature had only a weak effect on film cristallinity. All types of sensors showed good thermal stability. No change in film morphology was observed after CO sensing measurements. Moreover, the electrochemical impedance spectroscopy (EIS) measurements were investigated to better understand the nanostructured mixed metal oxide properties.

5.2 Introduction

Metal-oxide semiconductor films have been widely studied as sensors for pollutant gases [1-5]. Some of them show a significant change in conductivity upon exposure to different gases such as O_2, CO, H_2, etc [1, 2, 5-8]. In particular, isostructural single oxides such as TiO_2 and SnO_2 have been investigated and also commercialized for harmful gas monitoring [2, 9-12]. However, in some crucial applications, such as combustion exhaust monitoring at high temperatures (above 500°C), the single oxide sensors showed poor performance. For example, at high temperatures, SnO_2 suffers from structure instability and poor selectivity, while

TiO_2-sensors show low sensitivity [10]. Therefore, the use of heterometallic oxides (mixed metal oxides or doped metal oxides) has recently emerged as promising for gas sensors because it is possible to combine the best positive sensing properties of each oxide [3, 7, 24-26].

In particular, SnO_2 mixed with TiO_2 has been observed to be a good combination due to their similar structures (rutile phase) and closed lattice parameters. The phase diagram for SnO_2-TiO_2 binary composition predicts an immiscibility domain, where favourable conditions are created for spinodal or chemical decomposition (formation between modulated phase and TiO_2 or SnO_2-rich phases) [27]. The substitution of Sn for Ti in the lattice structure in solid solution (spinodal region) is proven to aid the formation of solid solutions, alter the structure and contribute to the thermal stability of TiO_2 [13-18]. This may lead to an improvement in gas sensing properties.

On the other hand, it has been observed that doping with suitable cations with low bulk solubility can also modify the electronic properties for gas interaction on the exposed surface as a result of grain boundary and surface segregation [13, 14, 19, 28]. Previous results showed that substitution of cations, such as Nb, Ta or Cr, can enhance gas sensing properties of TiO_2 [29-32]. Nb-ions were found to affect the equilibrium reaction between the point defects in bulk of sensing materials, therefore the gas-sensor performance can be enhanced [29-32, 46-49]. Beside the effect of surface defects, Ta^{+5} or Nb^{+5} dopants can also reduce the number of oxygen vacancies, thus retarding the phase transition of TiO_2 from anatase to rutile [11, 29, 46-47].

Moreover, the physical properties of a gas sensors can be improved by reducing the size of metal oxides to a nano-meter scale [5]. One reason is that the surface-to-bulk ratio for the nano-sized metal oxides is much larger than that of bulk metal oxides, leading to an enhancement of surface properties. Another reason is that the conduction type of the metal oxide is determined by grain size. When the grain size (D) is small enough ($D < 2L$, L is the space-charge depth), the metal oxide resistivity is determined by grain control and the conduction becomes a surface

conduction. Thus, grain-size reduction becomes one of the main factors in enhancing the gas sensing properties of semiconducting oxides [33-35].

Thus, the aim of this work is an attempt to merge both the advantages of mixed metal oxides and nanocrystalline materials for better sensing properties of gas sensors. Typically, precipitation, sputtering techniques and mostly sol-gel techniques were used to synthesize nano-structured heterometallic oxides [33, 36-40, 42]. Among those techniques, our previous studies showed interesting results using the microemulsion of anionic surfactant for synthesizing nanostructured Nb-doped TiO_2 [30, 41]. However, NaCl needs to be added to the system to control the microstructure of reverse micelles. This leads to a difficulty for synthesizing complex systems of mixed metal oxides (more than three metal oxides) and sometimes causes impurity in the synthesized powder. Thus, in this study, the microemulsion system of nonionic surfactant (TX-100) was used instead of ionic surfactant, AOT [41] and was addressed as an alternative and as an effective method of synthesizing such complex types of metal oxides, i.e. Nb-doped TiO_2 (TN) and SnO_2 mixed with Nb-doped TiO_2 with 2 different ratios: 10 to 1 (TSN 101), and 1 to 1 ratio (TSN 11). The nanostructured metal oxides were characterized and the sensing properties are presented.

5.3 Experimental

5.3.1 Metal Oxide Preparation

High purity nonionic surfactant, Triton X-100, and 1-hexanol (+98 %) were obtained from Fluka (Switzerland). The analytical reagents (AR), consisting of 99.0 % cyclohexane as an oil phase and 99.5% acetone, were purchased from Lab-Scan (Thailand). Ammonium hydroxide (NH_4OH, AR grade) was purchased from J.T.Baker (N.J., U.S.A.), and niobium (V) chloride and tin (IV) chloride pentahydrate from Sigma-Aldrich (Germany). Titanium dioxide (TiO_2, P25) was obtained from Degussa (Frankfurt, GmbH) and 40% hydrofluoric acid (HF) from Riedelde Haën AG. Perchloric acid (56%, $HClO_4$) was purchased from Carlo Erba (Italy). Hydrochloric acid (36.46 % wt, HCl) was obtained from VRW (England). All

reagents were used without further purification. Deionized water was used throughout the experiments.

Titanium tetrachloride solution ($TiCl_4$) in concentrated HCl was prepared by dissolving and heating TiO_2 in concentrated aqueous HF solution until a clear solution was obtained. Then a few milliliters of $HClO_4$ was added to remove excess HF from the solution. Finally, titanium tetrachloride in concentrated HCl solution was obtained by adding HCl. The reactions are:

$$TiO_2 + 4HF \rightarrow TiF_4 + 2H_2O \quad (5.1)$$

$$2TiF_4 + HClO_4 + 7HCl \rightarrow 2TiCl_4 + 4F_2 + 4H_2O \quad (5.2)$$

The oil phase was prepared by mixing 66.78 g of TX-100 and 53.00 g of *n*-hexanol with 210.33 g of cyclohexane. Then the solution was mildly stirred for 30 minutes. For the aqueous phase, the preparation was performed under N_2 atmosphere. The aqueous phase was prepared by weighing (g) $NbCl_5$ and (g) $SnCl_4$ pentahydrate followed by the addition of 10 ml of 36.46% wt of HCl and 5 ml of 1.6 M $TiCl_4$ and then adding deionized water until 25 ml of solution was obtained (Table 5.1). After the addition of 3.84 ml of aqueous phase in the string oil phase, a microemulsion was formed in a few seconds, which was indicated by a clear solution. Then, the microemulsion was continuously stirred and equilibrated at 30°C for 1 day. The obtained microemulsion was separated for precipitation in the controlled system fixed at 30°C. Then, precipitation was carried out by bubbling ammonia, prepared by bubbling air through a concentrated NH_4OH solution, into the microemulsion. The as-synthesized mixed oxide was separated by high-speed centrifuge at 10,000 rpm. It was then washed with cyclohexane, twice with ethanol and acetone, and finally by water to remove the remaining surfactant from the as-synthesized particles. The as-synthesized mixed oxide was dried and calcined for 5 h at 650°C.

5.3.2 Sensor Fabrication

Thick-film sensors were fabricated by suspending mixed oxide powders, TN, TSN 101 and TSN 11, with printing oil and depositing the resulting

slurry on an alumina substrate with comb-type Au electrodes. TN was fired at 650°C, TSN 101 was fired at 650°C and 850°C and TSN 11 was fired at 650, 750 and 850°C.

5.3.3 Materials Characterization

The phase analysis of the powders was performed by using an X-ray diffractometer (XRD, Phillips X-Pert Pro 500) at room temperature. Peak positions were compared with the standard files to identify crystalline phases. The size and shape of particles were observed using a transmission electron microscope (TEM, Jeol 2010, Tokyo, Japan). The Brunauer-Emmett-Teller (BET) specific surface area of TiO_2 was measured by using a surface area analyzer (Autosorb I, Quanta Chrom, U.S.A). The powders were first outgased to remove moisture and volatile adsorbates under vacuum at 300°C for 3 h before starting the analysis to determine the surface area. An Autosorb ANYGAS Version 2.10 was used to analyze the results. The effect of firing temperatures on the phase transformation of metal oxide films on alumina substrates was studied by grazing angle XRD-thin film mode and the morphology of the films was observed by field emission scanning electron microscopy (FE-SEM Leo Supra 35).

5.3.4 Gas Sensing Measurements

The gas sensing characteristics were examined in a conventional gas-flow apparatus equipped with a controlled heating facility. The sensors were alternatively exposed to air or CO (20-1000 ppm in air) at the total flow rate of 200mL/min, at 550°C. The films were left under 550°C with 5 mL/min air flow rate overnight before sensing CO. After CO was applied into the flow system, an increase in conductivity of metal oxides was observed and thus an increase in current was detected. The step response was observed by switching the flow from air to gas and gas to air. The gas response is defined as the ratio of R_{air}/R_{gas} where R_{air} and R_{gas} are the resistances in air and under gas exposure, respectively.

Impedance measurements were performed in a frequency domain between 0.01 and $1 \cdot 10^7$ Hz using a Frequency Response Analyzer Solartron 1260. The impedance study of TSN 11 and TSN 101 films was carried out at 550°C, the

same temperature that was used for dc gas measurements. The sensors were exposed to both oxidizing and reducing gases (1000 ppm CO in air, O_2, air, and 1000 ppm NO_2 in air).

5.4 Results and Discussion

5.4.1 Structural and Microstructural Analysis of TiO_2 Powder

Results obtained for pure TiO_2 and Nb-TiO_2 prepared using microemulsions have been reported in previous papers [30, 41]. Briefly, pure TiO_2 clearly showed a phase transformation from anatase to rutile structure at 650°C while Nb-TiO_2 was presented in anatase phase even at 850°C. In comparison with previous results of pure anatase, the XRD patterns of Nb-TiO_2 (TN), low loading SnO_2 mixed Nb-TiO_2 (TSN 11) and high loading SnO_2 mixed Nb-TiO_2 (TSN 101) powders were investigated at 650°C (Figure 5.1). The XRD pattern of TN showed no phase transition from anatase (2θ= 25.7) to rutile (2θ = 27.5) structures at 650°C. This result confirmed the effect of Nb stabilizing anatase structure, which agreed well with the relevant literature [41, 46-49]. For TSN 11 and TSN 101, no rutile phase was observed as well. In addition, beside the anatase structure, it was found the peak of a mixed solid solution between rutile structure of SnO_2 and TiO_2, at 2θ between 26.5 and 27.5 (plane 110). The effect of temperature on the phase transition will be later carefully observed at higher temperature (650°, 750° and 850°C) when the powder was used for sensor film preparation.

From XRD data, the crystal size of powders was determined using the Scherrer formula. The 2 theta at 25.7 was used in case of TN and the peak between 26.5-27.5 was used in case of TSN 101 and TSN 11. The results are shown in Table 5.2. The finest crystallite size of 19 nm was obtained for TSN 11, while the largest (at 650°C) crystal size of almost 44 nm was obtained for TSN 101.

The results of TEM observations indicated that TN featured an almost uniform morphology in anatase structure (with the characteristic plane 101 of 3.52 Å) (Figure 5.2). The average crystal size was about 14 nm. For TSN 101, there were

two different mean crystal sizes, 50 nm and 10 nm. Moreover, high resolution TEM revealed a shift in d-spacing of this mixed oxide sample between rutile structure of TiO_2 and SnO_2 (characteristic plane 110, d =3.25 Å), which also agreed well with the XRD pattern of powder (Figure 5.3). For high loading SnO_2 mixed Nb-TiO_2 (TSN 11), the results showed very fine and uniform powder with the mean crystal size of 10 nm. High resolution TEM also revealed both anatase phase (d = 3.52 Å) and the mixed solid solution phase at a shift in d-spacing of 3.3 Å (Figure 5.4). The larger the atomic ratio of Sn to Ti, the larger the d-spacing observed. This shift indicated the solid solution between TiO_2 and SnO_2 [16-17, 38]. The formation of both anatase phase and solid solution can be explained, as indicated in the literature [16-17, 38], because chemical decomposition (formation between the modulated phase and TiO_2 or SnO_2-rich phases) can occur if the condition does not favour thermodynamic or equilibrium conditions, which can easily occur in the fast precipitation (less than 60 seconds) of the microemulsion environment.

Table 5.3 shows the overall properties of the synthesized mixed oxide powders. The finest crystal size was obtained for TSN 11, while the largest crystal size and the most various mean crystal sizes were obtained for TSN 101. The differences in mean crystal size of mixed oxide may corresponded to the kinetic of precipitation in micro-environment of reverse micelles. Even though the kinetics of precipitation is hard to observe, the literature suggested that the higher metal concentration affected the higher amount of nucleus formation, thus the metal oxide size decreased [57]. In the experiments, the concentrations of $TiCl_4$ and $NbCl_5$ were kept constant while $SnCl_4$ concentration was varied at 0.15 and 1.5 M for TSN 101 and TSN 11, respectively. Thus, the total metal concentration was increased with an increase ratio of Ti to Sn. Therefore, the smaller size of crystal was observed for TSN 11. However, the crystal size of TSN 101 is higher than those obtained for TN even though the total metal concentration was higher. This might due to the different concentrations of Sn and Ti ions present in the aqueous phase, resulting in a different thermodynamic of nucleation and growth rate. Thus, two different mean crystal sizes at 10 and 50 nm were obtained in the case of TSN 101.

Mixed SnO_2 into 3% at. Nb-TiO_2 (TSN 11 and TSN 101) can cause a small decrease in BET surface area. The surface area of TSN 11 was slightly lower than TN even the crystal size was smaller. This might correspond to Sn mixed into TiO_2 leading to a dense phase of solid oxide, even the crystal size were about the same.

5.4.2 Structural and Microstructural Analysis on Thick-Film Sensors

Figure 5.5 shows the XRD patterns of TN, TSN 101 and TSN 11 film after firing sensor film at 650°C, and for sake of comparison, single oxide (SnO_2) and physically mixed SnO_2 with Nb-doped TiO_2 sample obtained from the microemulsion technique by mixing the two oxides with the 1 to 1 atomic ratio (SnO_2/TiO_2). In addition, since the thin film technique was used to verify the phase of mixed oxide on the alumina substrate, the reference pattern of the alumina substrate without coating the sensor film was examined and is shown in Figure 5.5 (f) as a reference pattern.

In case of TN, the XRD plot showed only anatase structure of TiO_2. (Figure 5.5, d). This result agreed well with our previous study of the use of anionic surfactant system of microemulsion for Nb-doped TiO_2 preparation, TEM result and also with the literature [30, 48, 44-45]. The anatase stabilization is due to the effect of Nb^{+5} substituting Ti^{+4} in the crystalline lattice, which reduced the number of oxygen vacancies, thus retarding the anatase-to-rutile transformation and grain growth. The crystal size of all the films was also determined using the Scherrer formula, but there were no significant changes in crystal size of the samples after firing.

The XRD of the film also show the same trend as that of the XRD patterns of the powders. Nb can stabilize anatase structure of TN, TSN 101 and TSN 11. The XRD pattern of TSN 101 and TSN 11 indicated both an anatase phase (2θ , = 25.3) and a solid solution phase of TiO_2 mixed with SnO_2 (2θ , = 26.5 - 27.5, plane 110). The results of TSN 11 and TSN 101 (Figure 5.5, a and b) indicated a distinct XRD pattern between the single oxide SnO_2 (Figure 5.5, e) and mixed SnO_2/TiO_2 from external mixing (Figure 5.5, c). The results also agreed well with the

literature [16-17, 38]. There is no solid solution for the mixed SnO_2/TiO_2; only the peak of each single oxide was shown separately. For high temperature obsevation, the anatase phase and solid solution were still maintained even when the sensing film was fired at 850°C [30] (Figure 5.6, a-c).

SEM results (Figure 5.6, a-c) showed thick film morphology of TN, TN 101, and TN 11, respectively, before exposure to CO. All the films were porous. TN and TSN 11 films presented very fine and uniform features. However, TSN 101 showed two different grain sizes. This may correspond to the two different phases of mixed oxide (anatase and solid solution), which also can be observed from TEM. The film morphology of Sn mixed Ti (TSN 11 and TSN 101) presented a denser morphology than those obtained from TN. This might be a cause of a decrease in surface area when Sn was mixed with TiO_2. Moreover, the morphology of all thick films after exposure to CO is shown in Figure 5.7 (a) to (c). The results indicated that all films presented no changes in grain size after long exposure to CO gas at 550°C for TN and TSN 11. However, the grain size was slightly increased in the case of TSN 101 (Fig. 5.8)

5.4.3 CO Sensing Response

Figure 5.9 shows the comparison of the sensor response (TSN 11 (a), TSN 101 (b) and TN (c)) films fired at 650°C to different concentrations of CO at 550°C. For TN, the largest gas response was 1.6 and was obtained in the presence of 1000 ppm of CO. In comparison to our previous work on Nb-TiO_2 system synthesized using anionic surfactant [30, 41], the sensitivity of TN sensor is smaller. In the case of sensors based on powders obtained with anionic surfactants the gas response was 2.2 at the same temperature and gas concentration [30]. This fact can be explained with the smaller grain size, 6 nm, and thus with larger surface area of these powders compared to the mean grain size, 14 nm, of TN powders.

Figure 5.9 (b) shows the CO response at 550°C of the TSN 101 film fired at 650°C. The results showed a good gas response at all gas concentrations. The largest was 4.3 and was measured at 1000 ppm of CO. This value is more than 3 times larger than the gas response obtained for the TN films. Even though the grain

size of TSN 101 was larger than TN, the gas response of TSN 101 sensor was higher. This might be due to the effect of the additional phase (the mixed solid solution structure) of mixed oxide that enhance the gas response of a pure anatase structure.

Figure 5.9 (c) shows the gas response at 550°C of the TSN 11 film fired at 650°C. A fast and large gas response to different CO concentrations was obtained. The highest value was almost 9 and was obtained at 1000 ppm of CO. This value is almost 7 times larger than that of TN film. Because of this very good gas response, the lower gas concentration range (20-100 ppm of CO in air) was examined and the results are shown in Figure 5. 10. It was found that the TSN 11 film still showed a gas response of 1.5 for a concentration of 20 ppm of CO. This best sensitivity is in accordance with the very fine and uniform grain size of TSN 11 film as shown in Figure 5.11. In order to study the effect of firing temperature on the gas response of the films, TSN 11 sensors were heated up at 750°C and 850°C. An increase in the gas response with the increase of the firing temperature was observed at all different gas concentrations. In Figure 5.12, the sensor response at 550°C of TSN 11 sensors fired at 650, 750 and 850° in the concentration range between 20 and 1000 ppm of CO was reported . The highest gas response, almost 10, was found for the film fired at 850°C in the presence of 1000 ppm of CO. The SEM images, showed in Figures 13, confirmed that the morphology of the film fired at 850°C has not changed and the grain size was still in nano-meter scale before and after the gas measurements at 550°C.

The best CO response was obtained for TSN 11 films. These results are in accordance with the structural and microstructural investigations. Moreover the firing temperature of the sensors was optimized at 850°C, allowing a very good gas response.

In order to highlight the improvement of the sensor performance using a combination of single metal oxides such as Nb-TiO2 and SnO2 rather than a single oxide, SnO_2 was synthesized using the same condition and system of noionic surfactant. SnO_2 sensors were prepared and fired at 650°C. A comparison between the gas response of SnO_2 and TSN11 sensors was performed. Moreover the gas

response of TSN 11 obtained from microemulsion was also compared to the response of TSN 11 obtained simply mixing the two single oxides in the 1:1 weight ratio. Both TNS 11 sensors were fired at 850°C. Figure 5.13 shows the gas response to 1000 ppm of CO at 550°C of SnO2, TSN 11 obtained from micromulsion and mechanically mixed TSN 11 sensors, respectively. The gas response of TSN 11 based sensors obtained from microemulsion was the highest and the more stable. The gas response of TSN 11 is almost 2 times the response of TSN 11 obtained by mixing the two oxides. This is further evidence that the solid solution phase observed in TNS 11 obtained by microemulsion may enhance CO response and thermal stability.

In order to better understand the nanostructured mixed metal oxide electrical properties, electrochemical impedance spectroscopy (EIS) measurements were performed. The impedance measurements on TSN 11 and TSN 101 sensors at 550°C in the presence of different atmospheres (air, O_2, 1000 ppm of CO and NO_2) are reported in Nyquist representation in Figures 5.14 and 5.15, respectively. In both cases, at high frequency a depressed arc followed by a not well-defined arc and linear behaviour at low frequency were observed. Both for TSN 11 and TSN 101 sensors, the high frequency semicircle increased (decreased) in the presence of an oxidizing (reducing) gas. Thus, the total resistance of the sensors increased in the presence of NO_2 and decreased in the presence of CO, in accordance to the behaviour of an n-type semiconductor and to the dc-voltage gas response previously reported. No significant difference was observed in the impedance spectra in air and in pure O_2. The high frequency semicircle can be interpreted with the classical series circuit of two parallel resistance-constant phase elements (CPE). According to the literature [50-56], only one semicircle is found for the nanometric ceramics, because bulk and blocking grain boundary responses overlap. The low frequency contributions are due to electrode reactions, in particular the linear behaviour can be attributable to the electrode polarization. This is in accordance to the low ionic conductivity at high oxygen concentration and low temperature of anatase phase of titania claimed by some authors [50-54]. It must also be taken into account that the sensors are made of very porous powders deposited on gold electrodes. Moreover, the linear behaviour at

low frequency is more evident for the TSN 101 sensor (Fig. 5.15) which contains a larger amount of doped titania in comparison to tin dioxide that is definitively a pure electronic conductor.

5.5 Conclusions

Reverse micelle microemulsion of a nonionic surfactant (brine solution/1-hexanol/Triton X-100/cyclohexane) was sucessfully used to synthesize nanostructured mixed metal oxides Nb-doped TiO_2 (TN) and SnO_2 mixed with Nb-doped TiO_2 in two 2 different ratios: 10 to 1 (TSN 101) and 1 to 1 ratio (TSN 11) respectively TN was found to have the highest surface area with only anatase phase with a mean crystal size of 14 nm. On the other hand, TSN 101 and TSN 11 had less surface area with two mixed phases (solid oxide and anatase). TSN 101 showed various crystal sizes of 10 and 50 nm while TSN 11 had a very fine and uniform mean crystal size of 10 nm. The morphology and phases of nanostructured mixed oxides have a significant effect on CO gas sensing. It was found that the sensitivity of TSN 11 was clearly the highest (about 11). This might be due to the combination effect of mixed solid oxide solution with the very small grain size and high thermal stability of TSN 11. For, TSN 101, although the solid solution was also present, the sensitivity was lower. This might be due to various grain size of powder. However, all types of films presented good thermal stability. No change in film morphology was observed before or after CO measurement. Therefore, in order to improve the properties of metal oxides, not only the gain size can play an important role, but also the phase and thermal stability of powder, which can be achieved by the right combination of mixed metal oxide powder.

5.6 Acknowledgements

This work was financially supported by the Golden Royal Jubilee Program, the Thailand Research Fund The authors would like to express sincere thanks for

National Metal and Materials Technology Center, Thailand for characterization using TEM and University of Rome "Tor Vergata" for help and support.

5.7 References

[1] S. S. Sunu, E. Prabhu, V. Jayaraman, K. I. Gnanasekar, T. K. Seshagiri, and T. Gnanasekaran, *Sensor. Actuators B*, **101**, 161-174 (2004).

[2] P. K. Dutta, M. Frank, G. W. Hunter, and M. George, *Sensors Actuators B*, **106**, 810-815 (2005).

[3] A. Ruiz, J. Arbiol, A. Cirera, A. Cornet, and J. R. Morante, *Mater. Sci. Eng-C*, **19**, 105-109 (2002).

[4] S. V. Patel, J. L., Gland, J. W. Schwank, K. D. Wise, and M. Zanini-Fisher, *Sensor. Actuat. B-Chem.*, **42**, 205-215 (1997).

[5] G. Martinelli, M.C. Carotta, E. Traversa and G. Ghiotti, *Mat. Res. Bull.*, **24**, 6, 30-36 (1999).

[6] K. R. Sharma and M. C. Bhatnagar, *Sensors Actuators B*, **56**, 215-219 (1999).

[7] J. Sheng, N. Yoshida, J. Karasawa, and T. Fukami, *Sensors Actuators B*, **41**, 131-136 (1997).

[8] J. Zhang, K. H. Au, Z. Q. Zhu, and S. Shea, *Opt. Mater.*, **26**, 47-55 (2004).

[9] M. Batzill and U. Diebold, *Prog. Surf. Sci.*, **79**, 47-154 (2005).

[10] P. I. Gouma, P. K. Dutta, and M. J. Mills, *Nanostruct. Mat*er., **11**, 1231-1237 (1999).

[11] M. C. Carotta, M. Ferroni, S. Gherardi, V. Guidi, and C. Malagù, *J.Eur. Ceramic. Soc.*, **24**, 1409-1413 (2004).

[12] L. Sun, L. Huo, H. Zhao, S. Gao, and J. Zhao, *Sensors Actuators B*, **114**, 387-391 (2006).

[13] J. R. Sambrano, L. A. Vasconcellos, J. B. L. Martins, M. R. C. Santso, E. Longo, and A. Beltran, *Theor. Chem.*, **629**, 307-314 (2003).

[14] F. R. Sensato, R. Custodio, E. Longo, A. Beltrán, and J. Andras, *Catal. Today*, **85**, 145-152 (2003).

[15] J. R. Sambrano, G. F. Nabrega, C. A. Traft, J. Andras, and A. Beltran, *Surf. Sci.*, **580**, 71-79 (2005).

[16] F. Edelma, H. Hahn, S. Seifried, C. Alfo, H. Hoche, A. Balogh, P. Werner, K. Zakrzewska, M. Radecka, P. Pasierb, A. Chack, V. Mikhelashvili, and G. Eisenstein, *Mat. Sci. Eng. B-Solid*, **69**, 386-391 (2000).

[17] C. Wang, B. Q. Xu, *J. Solid State Chem.*, **177**, 3448-3453 (2004).

[18] M. Radecka, P. Pasierb, K. Zakrzewska, and M. Rakas, *Solid State Ionics.*, **119**, 43-48 (1999).

[19] J. Oviedo and M.J. Gillan, *Surf. Sci.*, **490**, 221-236 (2001).

[20] Z. Zhang, H. Geng, L. Zheng, and B. Du, *Appl. Catal. A-Gen.*, **284**, 231-237 (2005).

[21] J. Zhang, Q. Li, and W. Cao, *J. Mater. Sci. Technol.*, **21**, 191-195 (2005).

[22] Z. Liu, K. Pan, M. Wang, M. Liu, Q. Lan, Y. Bai, and T. Li, *J. Photochem. Photobiol. A-Chem.*, **157**, 39-46 (2003).

[23] J. E. Kroeze and T. J. Savenije, *Thin Solid Film*s, **451**, 54-59 (2004).

[24] K. R. Sharma, M. C. Bhatnaga, and G. L. Sharma, *Sensors Actuators B*, **45**, 209-215 (1999).

[25] H. Zou and Y. S. Lin, *Appl. Catal. A- Gen.*, **265**, 35-42 (2004).

[26] A. M. Ruiz, A. Cornet, K. Shimanoe, J. R. Morante, and N. Yamazoe, *Sensors Actuators B*, **109**, 7-12 (2005).

[27] K. Zakrzewska, *Thin Solid Films*, **391**, 229-238 (2001).

[28] M. Radecka, K. Zakrzewska, and M. Rakas, *Sensors Actuators B*, **47**, 194-204 (1998).

[29] K. Zakrzewska, M. Radecka, and M. Rakas, *Thin Solid Films*, **310**, 161-166 (1997).

[30] T. Anukunprasert, C. Saiwan, and E. Traversa, *Sci. Technol. Adv. Mater*, **6**, 359-363 (2005).

[31] J. Marien, T. Wagner, G. Duscher, A. Koch, and M. Rühle, *Surf. Sci.*, **446**, 219-228 (2000).

[32] K. Zakrzewska, *Vacuum*, **74**, 335-338 (2004).

[33] O. K. Tan, W. Cao, Y. Hu, and W. Zhu, *Ceram. Int.*, **30**, 1127-1133 (2004).

[34] Y. Shimizu and M. Egashira, *Mat. Res. Bull.*, **6**, 18-24 (1999).

[35] N. Barsan and U. Weimar, *J. Electron. Mater.*, **7**, 143-167 (2001).

[36] N. Kanai, T. Nuida, K. Ueta, K. Hashimoto, T. Watanabe, and H. Ohsaki, *Vacuum*, **74**, 723-727 (2004).

[37] W. P. Tai and Jae. H. Oh, *Sensors Actuators B*, **85**, 154-157 (2002).

[38] O. K. Tan, W. Cao, Y. Hu, and W. Zhu, *Solid State Ion*ics, **172**, 309-316 (2004).

[39] L. Cao, H. Wan, L. Huo, and S. Xi, *J. Colloid. Interf. Sci.*, **244**, 97-101 (2001).

[40] Q. Liu, X. Wu, and B. Wang, *Mat. Res. Bull.*, **37**, 2255-2262 (2002).

[41] C. Saiwan, S. Krathong, T. Anukunprasert, and E. A. O'Rear (III), *J. Chem. Eng. Jpn.*, **37**, 279-285 (2004).

[42] M. A. Lopez-Quintela, *Colloid. Surf. Sci.*, **8**, 137-144 (2003).

[43] L. B. Kong, J. Ma, and H. Huang, *J. Alloy. Compd.*, **336**, 315-319 (2002).

[44] R. K. Sharma, M. C. Bhatnagar, G. L. Sharma, *Sensors Actuators B*, **46**, 194-201 (1998).

[45] E. Traversa, M.L. Di Vona, S. Licoccia, M. Sacerdoti, M.C. Carotta, M. Gallana, G. Martinelli, *J. Sol-Gel Sci. Technol.*, **22**, 167-179 (2001).

[46] M. C. Carotta, M. Ferroni, V. Guidi, and G. Martinelli, *Adv. Mater.*, **11**, 943-946 (1999).

[47] M. C. Carotta, M. Ferroni, D. Gnani, V. Guidi, M. Merli, G. Martinelli, M.C. Casale, and M. Notaro, *Sensors Actuators B*, **58**, 310-317 (1999).

[48] M. Ferroni, M.C. Carotta, V. Guidi, G. Martinelli, F. Ronconi, O. Richard, D. V. Dyck, and J. Van Landuyt, *Sensors Actuators B*, **68**, 140-145 (2000).

[49] N. Bonini, M. C. Carotta, A. Chiorino, V. Guidi, C. Malagù, G. Martinelli, L. Paglialonga, and M. Sacerdoti, *Sensors Actuators B*, **68**, 274-280 (2000).

[50] P. Knauth and H. L. Tuller, *J. App. Phys.*, **85**, 897-902 (1999).

[51] P. Knauth and H. L. Tuller, *Solid State Ionics*, **136-137**, 1215-1224 (2000).

[52] A. Weibel, R. Bouchet, and P. Knauth, *Solid State Ionics*, **177**, 229-236 (2006).

[53] Y. M. Chiang, E. B. Lavik, I. Kosacki, H. L. Tuller, and J. Y. Ying, *J. Electroceramics*, **1**, 7 (1997).

[54] I. Kosacki and H. U. Anderson, *Sensors Actuators B*, **48**, 263 (1998).

[55] J. P. Medeiros, E. C. de Souza Traveres, U. U. Gomes, and W. Acchar, *Ceramica*, **44**, 287-288 (1998).

[56] M. Koelsch, S. Casseignon, C. T. Minh, and J. P. Jolivet, *Thin Solid Films*, **86-92**, 451-452 (2004).

[57] I. Capek, *Adv. Colloid. Interf. Sci.*, ***110***, 49-74 (2004).

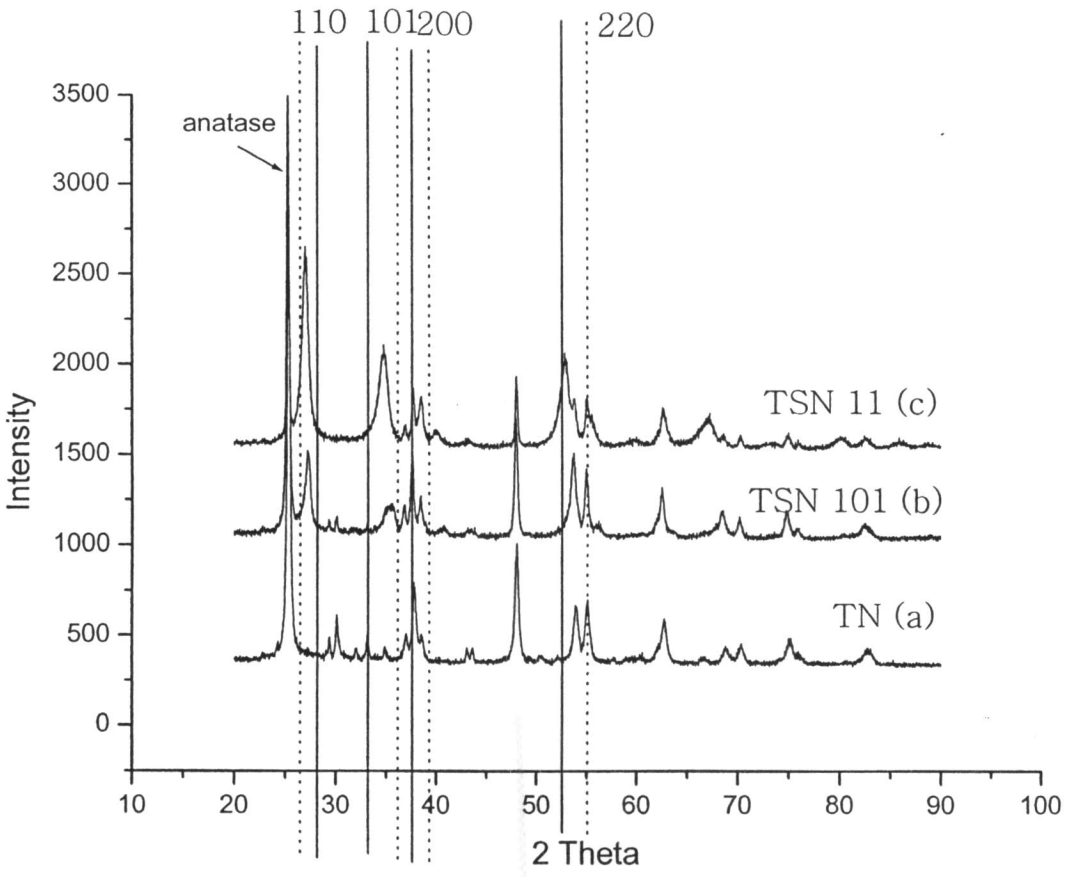

Figure 5.1 XRD pattern of TN (a), TSN 101 (b) and TSN 11 (c) powders calcined at 650°C.

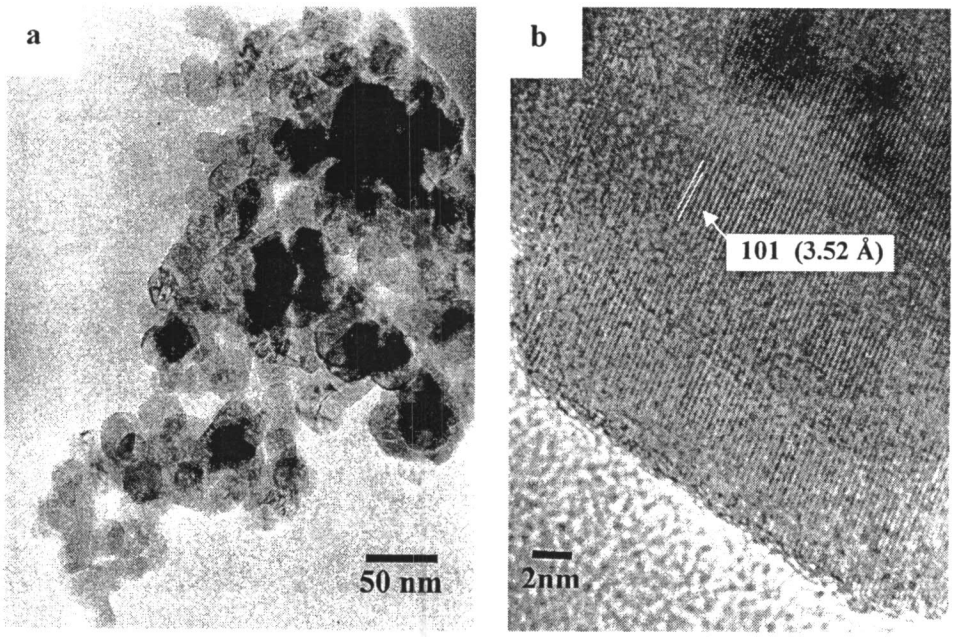

Figure 5.2 TEM image of Nb-TiO_2 powder (a) and the HR-TEM (b) of anatase structure (plane 101) of TiO_2 calcined at 650°C.

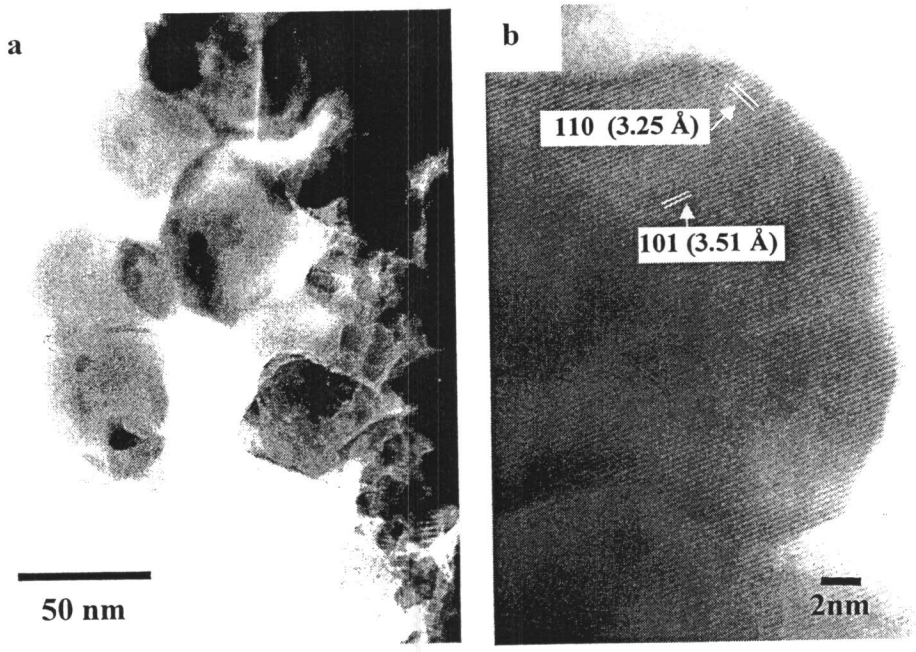

Figure 5.3 TEM image of TSN101 powder (a) and the HR-TEM (b) of solid solution of SnO_2 mixed TiO_2 calcined at 650°C.

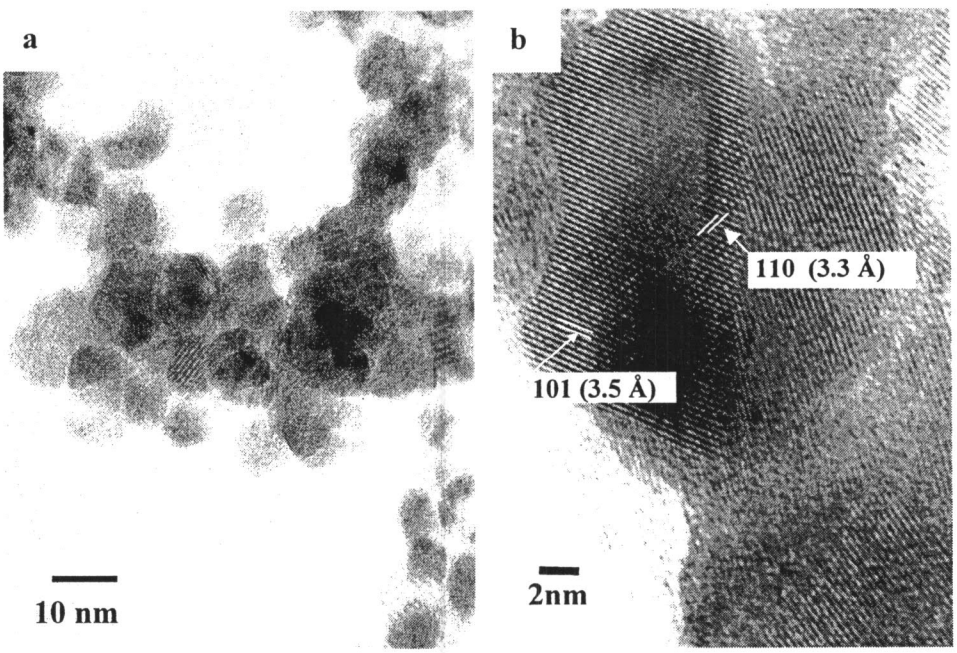

Figure 5.4 TEM image of TSN11 powder (a) and the HR-TEM (b) of solid solution of SnO_2 mixed TiO_2 calcined at 650°C.

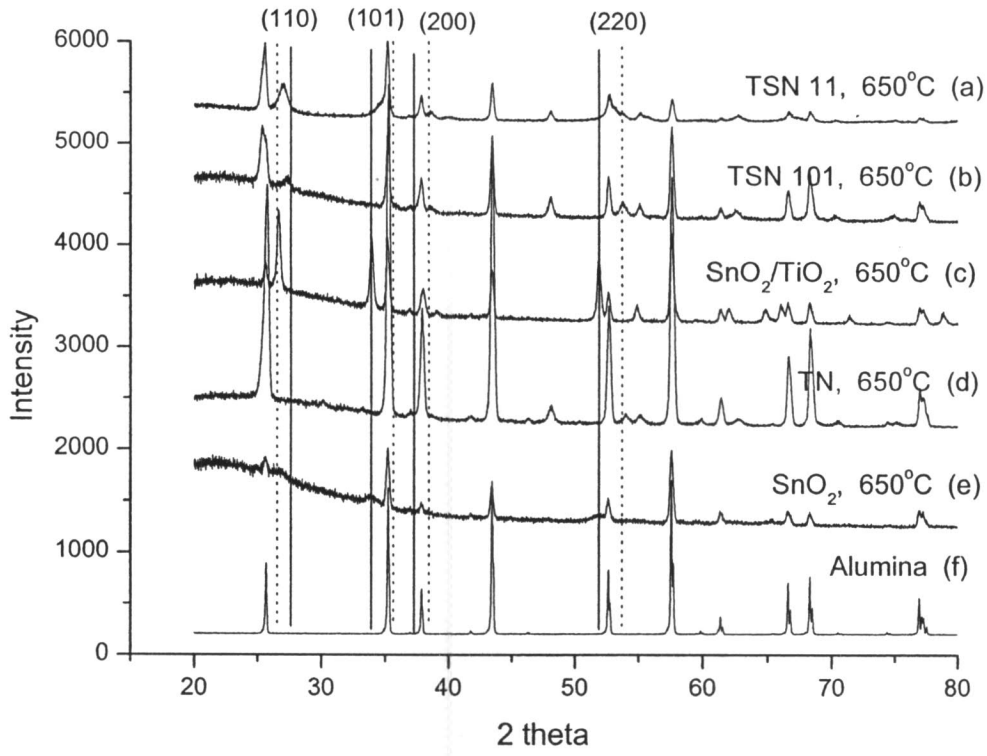

Figure 5.5 XRD patterns of films fired at 650°C; TSN 11 film (a), TSN 101 film (b), grained SnO_2 mixed Nb-TiO_2 with 1:1 ratio (c), Nb-TiO_2 (d), SnO_2 (e) and alumina substrate (f).

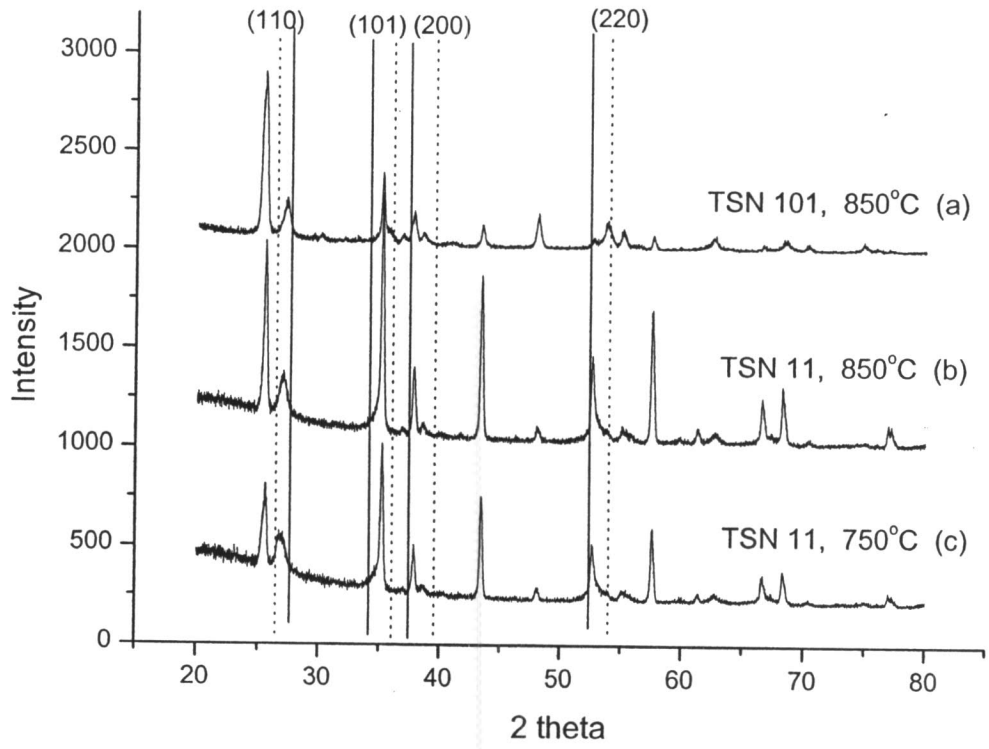

Figure 5.6 XRD pattern of; TSN 101 film fired at 850°C (a) and TSN 11 film fired at 750° (b) and 850°C (c).

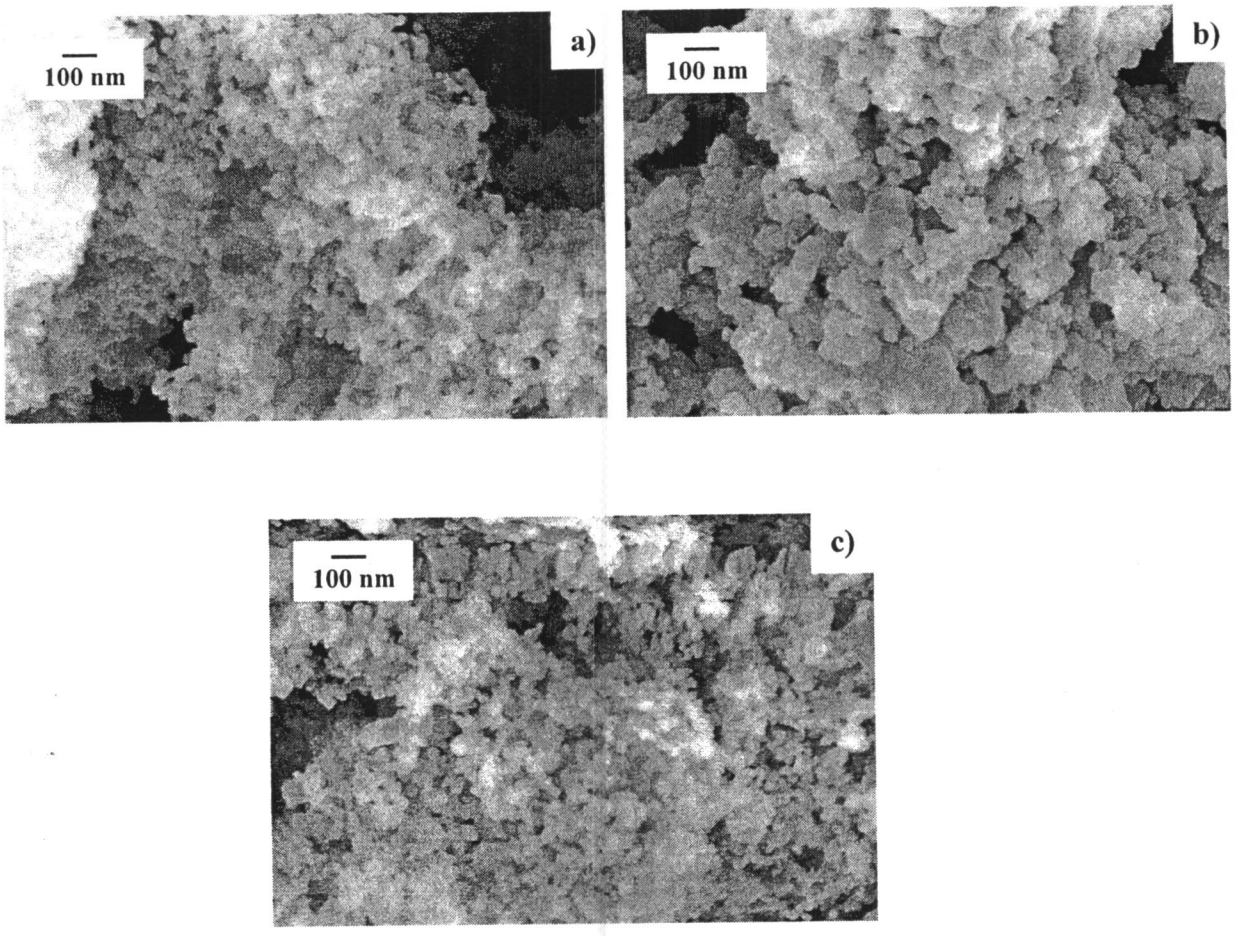

Figure 5.7 SEM picture from: TN sensor film (a); TSN 101 film (b); and TSN 11 film (c), fired at 650 °C before CO gas measurement.

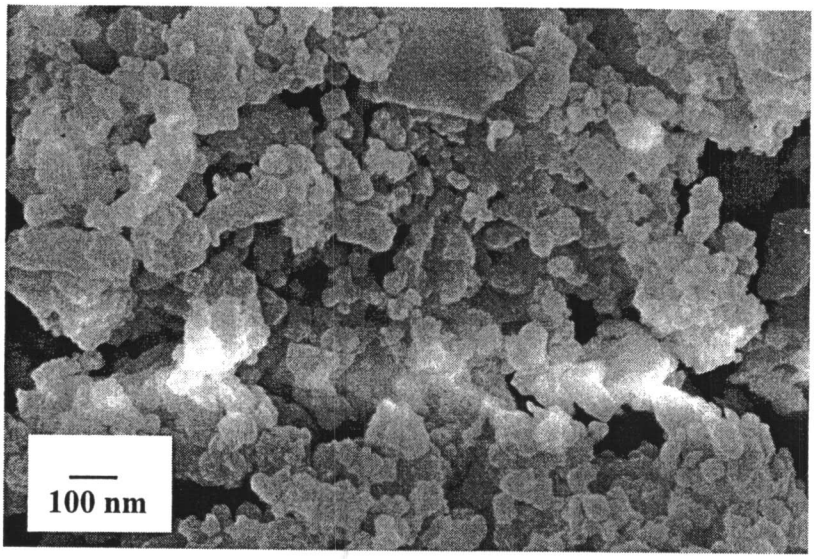

Figure 5.8 SEM picture from TSN 101 film after CO gas measurement.

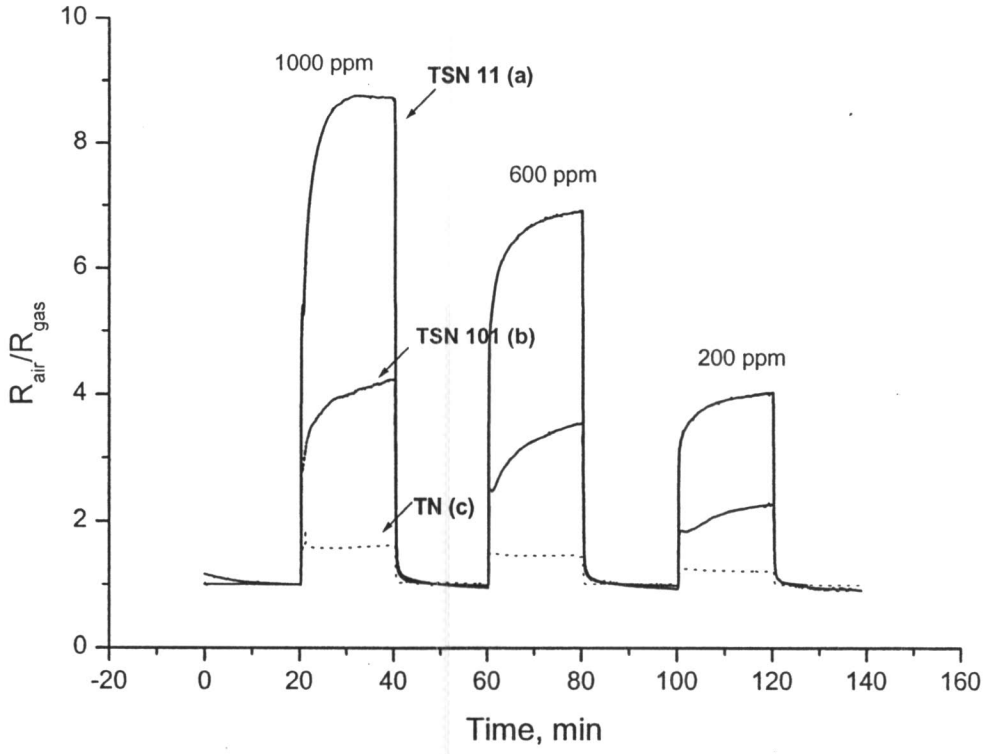

Figure 5.9 Sensor response of TSN 11 (a), TSN 101 (b) and TN (c) fired at 650 °C to 200-1000 ppm CO at 550°C with an applied voltage of 15 V.

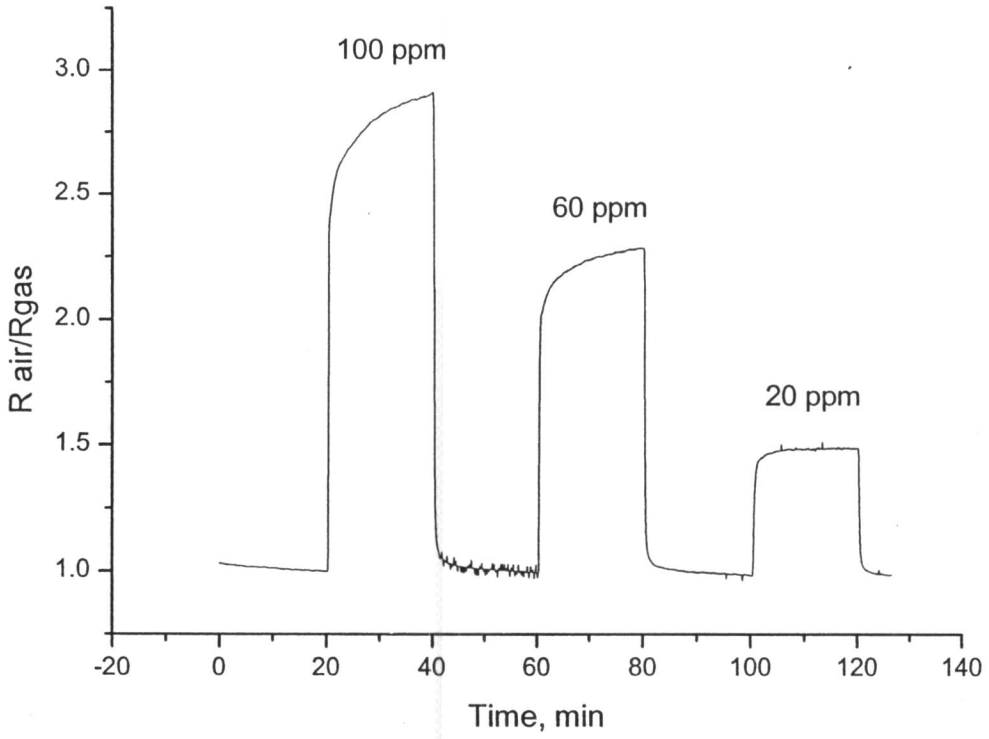

Figure 5.10 Sensor response of TSN 11 fired at 650 °C to 20-100 ppm CO at 550°C with an applied voltage of 15 V.

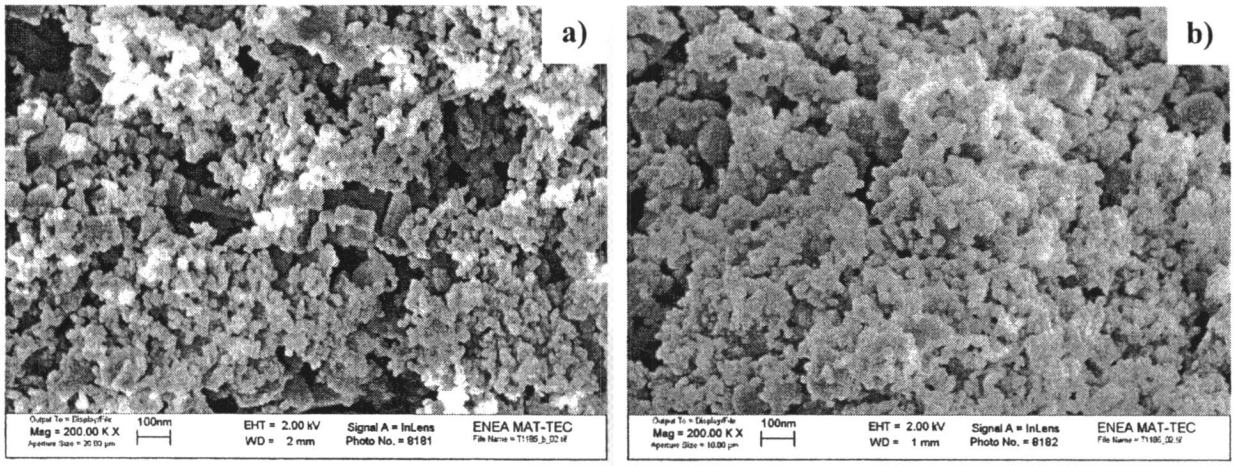

Figure 5.11 SEM micrographs of TSN 11 sensors fired at 850 °C a) before CO gas measurement and b) after CO measurement at 550°C.

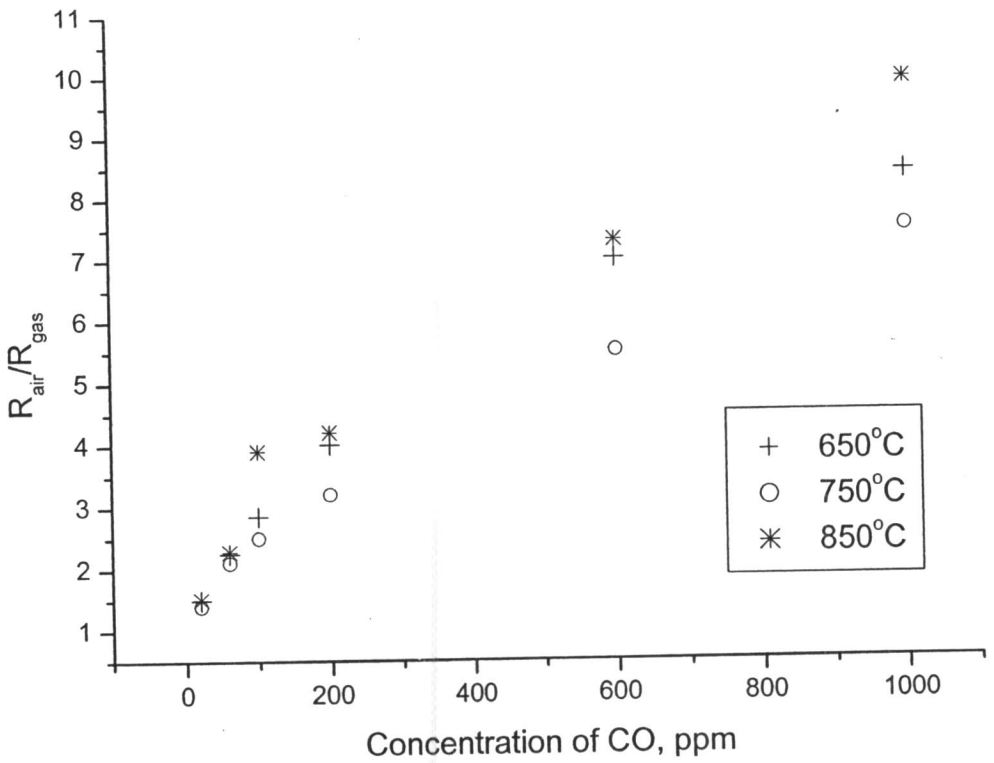

Figure 5.12 Sensor response of TSN 11 sensors fixed at 650°, 750° and 850°C in the 20-1000 ppm range of CO in air.

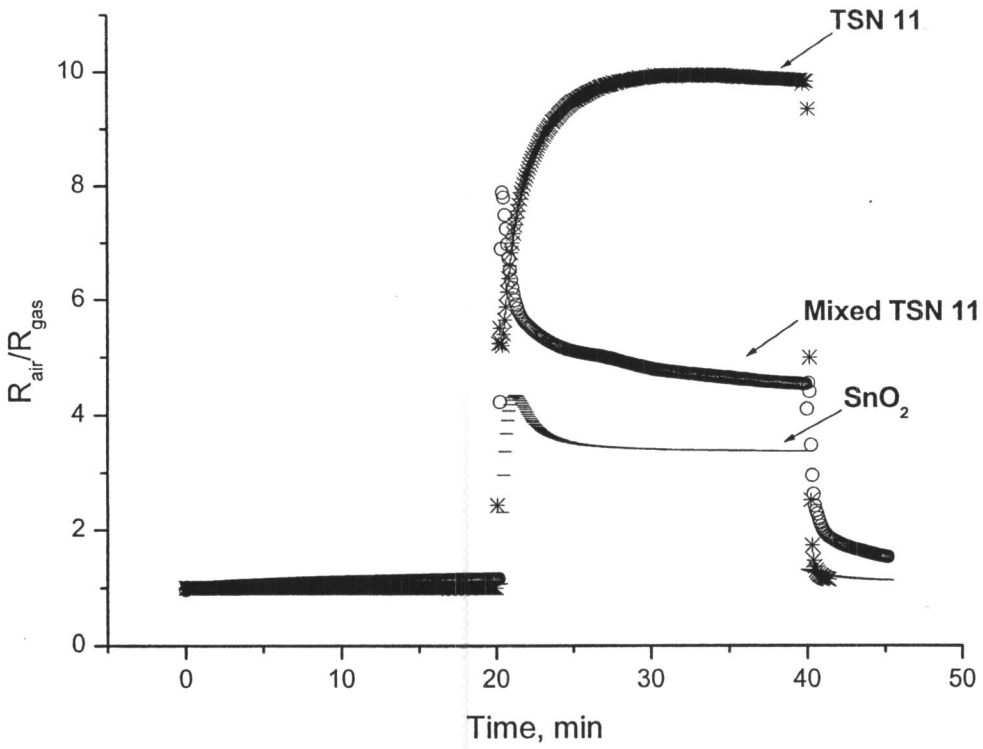

Figure 5.13 Comparison of gas response of SnO_2 fired at 400°C, mixed TSN 11 fired at 850°C, and TSN 11 prepared from microemulsion (TSN 11, ME) fired at 850°C. to 1000 ppm of CO at 550°C.

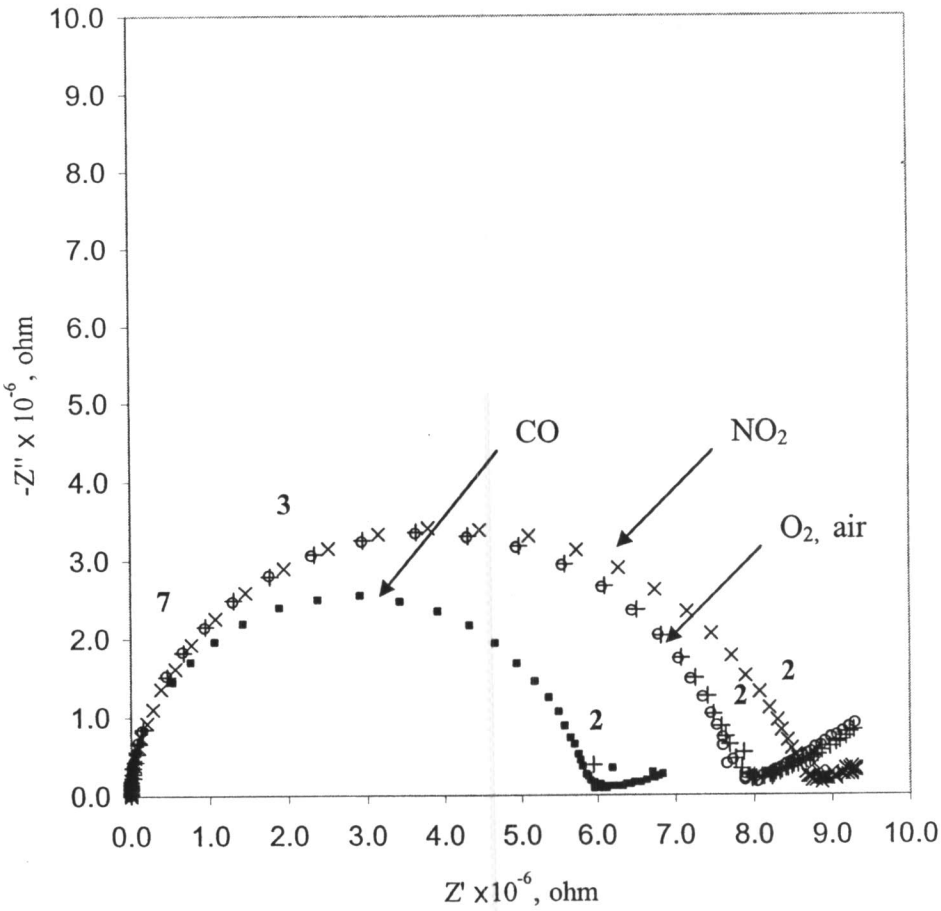

Figure 5.14 Nyquist plot of TSN 11 film fired at 550°C. The numbers above the spectra correspond to the logarithm of the measurement frequencies.

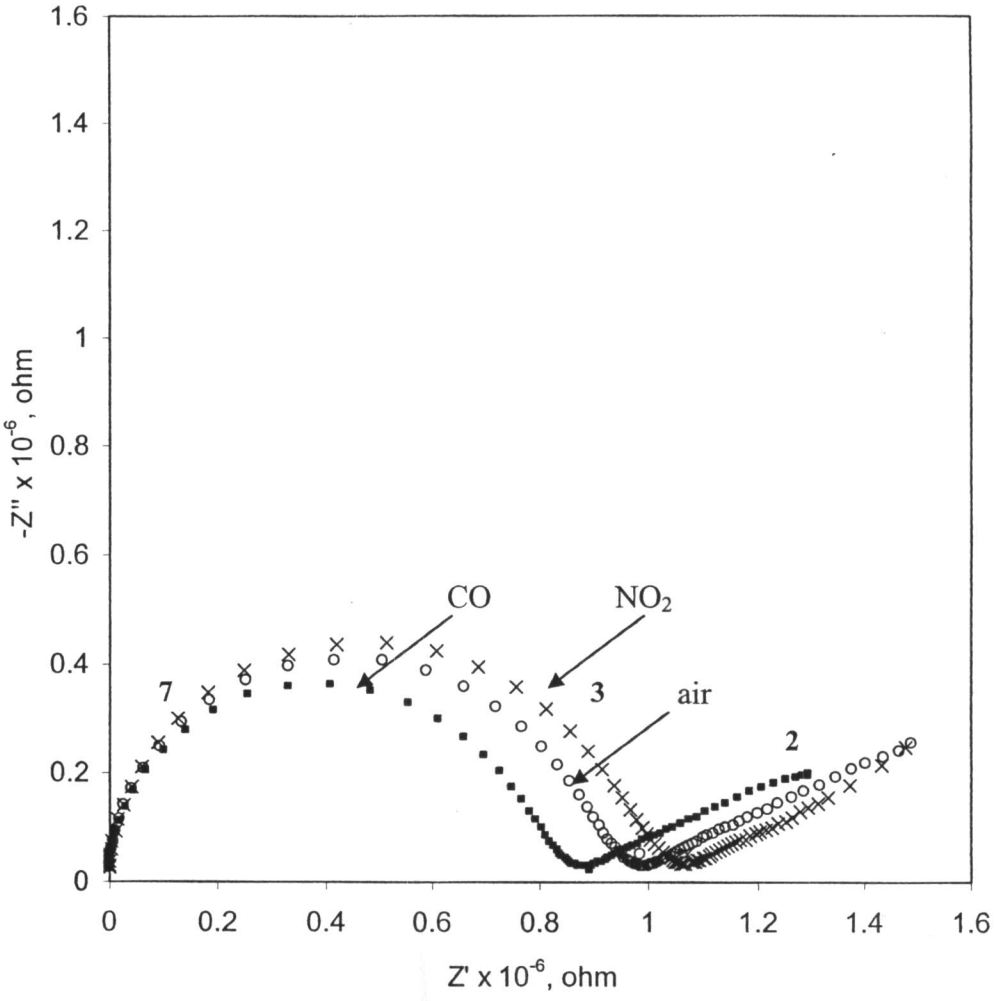

Figure 5.15 Nyquist plot of TSN 101 film fired at 550°C. The numbers above the spectra correspond to the logarithm of the measurement frequencies.

Table 5.1 Conditions for preparation of different atomic ratios of precursors*

Mixed metal oxide types	1.5 M of $TiCl_4$, (ml)	$SnCl_4$ (g)	$NbCl_5$ (g)
3%Nb-doped TiO_2 (TN)	5.0	-	0.06079
3%Nb-doped TiO_2 mixed with SnO_2 by ratio 1 to 1 (TSN 11)	5.0	0.26294	0.06079
3%Nb-doped TiO_2 mixed with SnO_2 by ratio 10 to 1 (TSN 101)	5.0	2.62935	0.06079

* All components were mixed in diluted HCl solution for preparation of 25 ml aqueous phase.

Table 5.2 Mean crystal size of powder determined by XRD using the Scherrer formula

Metal oxides	Mean crystal size (nm)
TN	16.4
TSN 11	13.1
TSN 101	37.6

Table 5.3 Overall properties of synthesized mixed oxide

Metal oxides	**Mean crystal size (nm)**	**BET surface area (m^2/g)**	**Phase**
TN	14	98	anatase
TSN 11	10	87	anatase and solid solution
TSN 101	10 and 50	68	anatase and solid solution